Journal of Applied Polymer Science

Microstructure and characterization of electrospun poly(vinyl alcohol) nanofiber scaffolds filled with graphene nanosheets

Chien-Lin Huang,[1] Sheng-Yin Peng,[1] Yu-Jyun Wang,[1] Wen-Cheng Chen,[1] Jia-Horng Lin[1,2,3]

[1]Department of Fiber and Composite Materials, Feng Chia University, Taichung 40724, Taiwan

[2]School of Chinese Medicine, China Medical University, Taichung 40402, Taiwan

[3]Department of Biotechnology, Asia University, Taichung 41354, Taiwan

Correspondence to: C. L. Huang (E-mail: clhuang@mail.fcu.edu.tw)

ABSTRACT: Graphene nanosheets (GNSs) have attracted significant scientific attention because of their remarkable features, including exceptional electron transport, excellent mechanical properties, high surface area, and antibacterial functions. Poly(vinyl alcohol) (PVA) solutions filled with GNSs were prepared for electrospinning, and their spinnability was correlated with their solution properties. The effects of GNS addition on solution rheology and conductivity were investigated. The as-spun fibers were characterized via scanning electron microscopy (SEM), transmission electron microscopy (TEM), wide-angle X-ray diffraction (WAXD), and differential scanning calorimetry (DSC). The results revealed the effects of GNS on the microstructure, morphology, and crystallization properties of PVA/GNS composite nanofibers. The addition of GNSs in PVA solution increased the viscosity and conductivity of the solution. The electrospun fiber diameter of the PVA/GNS composite nanofiber was smaller than that of neat PVA nanofiber. GNSs were not only embedded at the fibers but also formed protrusions on the fibers. In addition, the crystallinity of PVA/GNS fiber decreased with higher GNS content. The possible application of PVA/GNS fibers in tissue engineering was also evaluated. © 2015 Wiley Periodicals, Inc. J. Appl. Polym. Sci. **2015**, *132*, 41891.

KEYWORDS: biomedical applications; composites; crystallization; electrospinning; graphene

Received 30 September 2014; accepted 8 December 2014

DOI: 10.1002/app.41891

INTRODUCTION

Electrospinning technique has attracted increasing attention in recent years in the field of fabricating polymeric nanofibers. Nanofiber mats have shown considerable potential in tissue engineering and drug delivery because of their high surface area-to-volume ratio and structures that mimic extracellular matrix.[1] Poly(vinyl alcohol) (PVA) is widely used in various biomedical applications, such as wound dressings,[2] tissue scaffolds,[3] and drug release,[4] because of its solubility in water, biocompatibility,[4] and biodegradability at specific conditions.[5,6] Electrospun PVA nanofibers with diameters of 100 nm to 1000 nm have attracted considerable attention.[7,8] In addition, given that PVA can be easily dissolved in water, stabilizing PVA fiber structures against disintegration in water is important for tissue engineering applications. PVA polymer chains have to be cross-linked via physical or chemical methods to prevent the disintegration of PVA nanofibers in water. However, most PVA chemical cross-linking agents, including glutaraldehyde, acetaldehyde, and formaldehyde, are not appropriate for bioengineering because of their cytotoxicity.[9–11] Therefore, physical cross-linking is the optimal way to prevent PVA disintegration in water. The crystallinity of PVA nanofiber can perform a major function in decreasing water solubility.[11] Both academic and industrial interests have resulted in extensive studies on the physical cross-linking of PVA for medical and healthcare textiles.

More importantly, to improve the properties of PVA nanofiber scaffolds, different kinds of additives[3] and fillers[2,11–13] were added into electrospun PVA nanofibers. Song *et al.*[3] reported that PVA nanofibers filled with collagen and hydroxyapatite enhanced the adhesion and proliferation of murine bone cells. Hong *et al.*[11] found that PVA nanofibers filled with Ag nanoparticles showed extremely high antimicrobial activity. Naebe *et al.*[12] studied the structure–property relationships of PVA/single-walled carbon nanotube (SWCNT) composite nanofibers prepared via electrospinning. SWCNT induces the nucleation process of PVA crystallization.

Graphene fillers present outstanding electron mobility and mechanical properties, as well as a large surface area.[14] Thus,

Additional Supporting Information may be found in the online version of this article.

two-dimensional graphene nanosheets (GNSs) with thicknesses of several nanometers have become a great focus in various application areas and have been extensively studied, particularly in polymer composites. Recently, GNSs have been used to enhance antibacterial properties and accelerate cell differentiation in tissue engineering. Lu *et al.*[2] showed that GNS as an antibacterial material filler can be beneficial for wound healing in PVA/GNS composite nanofibers. Nayak *et al.*[15] found that GNS provides a promising biocompatible scaffold that does not hamper the proliferation of human mesenchymal stem cells and accelerates their specific differentiation into bone cells. Therefore, apart from improving the physical properties of host polymers for composites, GNSs also exhibit potential use in medical applications.

The large number of hydrophilic groups on graphene oxide (GO) imparts dispersability at the individual sheet level in water. Water is an ideal solvent to prepare electrospun PVA/GO composite nanofibers. In addition, Qi *et al.*[13] showed that PVA/GO nanofibers improved the adhesion and proliferation of mouse osteoblastic cells. However, Veca *et al.*[16] found that PVA was attached to GO via an esterification reaction between the carboxylic acid moieties on GO and hydroxyl groups on PVA. The viscosity of the PVA solution with high GO content is too high for electrospinning (Supporting Information Figure S1). Although the chemical reduction of GO still presents several flaws of GO, it can reduce the esterification reaction between GO and PVA and is a promising method to achieve mass production. Therefore, the higher addition of GNSs in PVA nanofibers results in higher electrospinning ability than that of GOs in PVA nanofibers.

To disperse GNSs in an aqueous solution, the nanosheets are sonicated in the presence of stabilizers such as sodium dodecylbenzenesulfonate (SDBS)[17–19] and poly(vinyl pyrrolidone) (PVP).[20] Zhao *et al.*[18] prepared PVA/GNS nanocomposites via an SDBS aqueous solution. Significant enhancements in the mechanical properties and crystallization behavior of PVA/GNS composites were observed at low GNS loading. Das *et al.*[20] prepared PVA/GNS nanofibers by electrospinning an aqueous solution of polyvinylpyrrolidone-stabilized GNS and PVA. GNSs significantly increased the thermal stability and crystallinity of fibers. However, only 0.5 wt % GNS was used in that study. Although literature is available on electrospun PVA/GNS nanofibers, little information is available on the effects of different amounts of GNS on electrospinning, solution properties, and microstructures.

To obtain a better understanding on manipulating electrified jets to produce fibers with small diameters, a systematic study of the effects of GNSs on solution properties and electrospinning process is necessary. In this study, GO is used as building block of graphite via Hummers method[21] and is based on the top-down approach. In accordance with the developing method used by Cao *et al.*,[22] our GNSs were prepared by reducing GO with hydrazine and then combining via lyophilization. In addition, a small amount of SDBS was used to stably disperse GNS in the PVA solution. The rheological and conductive properties of the prepared PVA/GNS solution were measured and correlated with the electrospinnability characteristics of the solution. In addition, the effects of GNS-filled solutions on processing parameters were investigated. The addition of GNSs in PVA nanofibers was studied to elucidate the effects of the filler and physical treatment on morphology, microstructure, and crystallization of the composite fibers. PVA/GNS nanofibers were also cultured with fibroblasts to evaluate cell attachment and proliferation at early stage for tissue engineering applications.

EXPERIMENTAL

GNS Preparation

Graphite powders (1000 mesh) were purchased from Homytech Auto Parts Co. GO was synthesized via Hummers method.[21] Graphite powder (1 g) was stirred with 25 mL of concentrated sulfuric acid (cooled) at 0°C. Potassium permanganate (3.5 g) was slowly added to the suspension at 0°C. After removing from ice bath, the mixture was stirred at 60°C for 6 h. Distilled water (25 mL) was then gradually added into the reaction vessel to maintain the temperature at < 100°C for 30 min. The mixture was further diluted with distilled water, and hydrogen peroxide was then added. GO particles were separated by via centrifugation. Distilled water was poured in the container with the particles, followed by ultrasonic treatment for 3 h. Ammonia was added to the GO solution, and an ammonia-modified GO solution was produced (pH = 10.6). The dispersed material was reduced with hydrazine at 80°C for 24 h to generate a GNS suspension. The GNS suspension was frozen in a refrigerator, followed by 72 h of freeze-drying (EYELA FDA-830) [22] to obtain GNS powders.

PVA/GNS Preparation and Solution Properties

PVA powders with a weight average molecular weight of 146,000 g/mol to 186,000 g/mol and 98–99% degree of hydrolysis were purchased from Aldrich Co. SDBS were purchased from Acros Organics. To prepare a homogenous PVA/GNS solution with varying amounts of GNSs (based on PVA polymer), a PVA/GNS composite with the required composition was prepared using the following procedure to ensure good dispersion of GNS in the prepared solution. The weighed GNSs were added in a distilled aqueous solution containing SDBS, which was then subjected to ultrasonic treatment for 3 h, resulting in 5 wt % SDBS relative to a GNS sample. The preweighed PVA polymer was then added and vigorously stirred for several hours at 80°C. PVA solution (10 wt %) was used to monitor the effect of GNS on the morphology of the as-spun fibers. A PVA solution (10 wt %) with different amounts of GNSs (based on the weight of PVA polymer) was then obtained.[23] In the present study, a 99/1 sample designation indicates the polymer-to-filler weight ratio. Solution conductivity properties (κ) were measured at 25°C by using a Consort conductivity meter (C832). The viscoelastic properties of solutions filled with GNSs were measured in a strain-controlled rheometer (ARES, TA Instruments) by using a cup-and-bob feature at 25°C.

Electrospinning Process

All of the prepared solutions were subjected to room temperature electrospinning, in which the needle size was $D_i/D_0/length = 0.63\,\text{mm}/0.53\,\text{mm}/2\,\text{mm}$, where D_i and D_0 are the inner and outer diameters of the needle, respectively. The

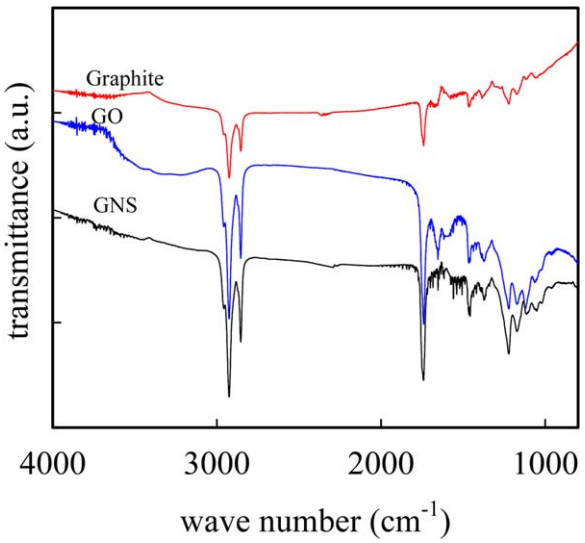

Figure 1. FTIR spectra of graphite, GO, and GNS. [Color figure can be viewed in the online issue, which is available at wileyonlinelibrary.com.]

prepared solutions were delivered by a syringe pump (Cole–Parmer) to the needle at a controlled flow rate (Q). High electrical voltage (V) was applied to the spinneret by using a high-voltage source (MECC, HVU-40P100) to provide sufficient electric field for electrospinning. To construct a needle-to-plate electrode configuration, an aluminum board (30 × 30 cm^2) was used as a collector for the electrospun fibers at a fixed tip-to-collector distance of 14 cm.

Morphology and Characterization of Nanofibers

The morphology of the fibers was observed using a scanning electron microscope (SEM, Hitachi S4100). Fiber diameters were measured from a collection of ~200 fibers, from which the average diameter (d_f) was determined. A transmission electron microscope (TEM, Jeol JEM-1200EX) was used to determine the locations of GNS particles within the nanofibers. WAXD patterns were obtained using a Bruker D8 Discover X-ray diffractometer with Cu K_α radiation to characterize the crystal lattice of the samples. Given the acquired WAXD intensity profile, peak deconvolution is required to estimate the relative content of PVA crystals. We tentatively used one broad peak at $2\theta \sim$ 20.3° for the amorphous phase. The crystalline peaks and amorphous halo were fitted with a Gaussian–Lorentzian area function. After peak deconvolution, the ratio of crystal amount was determined from the ratio of the integrated area of the PVA crystals. The crystallization and melting behaviors of the PVA/GNS nanofiber composites were investigated using a Perkin-Elmer DSC7 differential scanning calorimeter (DSC) in a nitrogen atmosphere at a 10°C/min scanning rate. Prior to measurements, indium and zinc standards were used to calibrate the enthalpies of fusion as well as the melting temperatures. The samples were heated to 240°C at a rate of 10°C/min. After holding at 240°C for 10 min, subsequent cooling was performed at a rate of 10°C/min.

Cell Abilities and Morphologies

Fibroblast (NIH 3T3, abbreviated 3T3) cells were provided by the National Institute of Health in Taiwan. 3T3 were derived from newborn mouse fibroblasts and cultured in Dulbecco's Modified Eagle's Medium (DMEM) (Gibco, Invitrogen Taiwan Ltd., MD) containing 10% bovine serum (Biological Industries, Haemek, Israel). The morphologies after cell proliferation culture on surfaces were examined at 72 h.

For the observation of cell morphologies on surfaces after cell culture, the samples were washed with phosphate-buffered saline (PBS) and fixed with a mixture of 2% paraformaldehyde and 2.5% glutaraldehyde for 2 h. After dehydration in a graded series of ethanol, the samples were treated with iso-amyl acetate and dried using a critical point dryer. The specimens were sputter-coated with gold, and cell morphology was observed via SEM.

RESULTS AND DISCUSSION

Characterization of GNSs

GO was prepared via Hummers method[21] by using 1000 mesh graphite flakes as the starting material in graphene preparation. After GO was allowed to react with hydrazine for 24 h, GO was reduced to GNS. Figure 1 shows the FTIR spectra of graphite, GO, and GNS. For graphite, two peaks are found at 2925 and 2854 cm^{-1}, which are assigned to methylene stretching, thereby illustrating the existence of CH_2 and CH groups. Moreover, graphite also shows small C=O stretching peaks for COOH at 1740 cm^{-1}. When the graphite was oxidized into GO, a broad new peak is found at around 3600 cm^{-1} to 3000 cm^{-1}, which is attributed to O–H stretching vibration. In addition, the peak intensity at 1740 cm^{-1} increased significantly and a new peak at 1662 cm^{-1} was formed, which is assigned to C=O in quinone.[24] The peak at around 1610 cm^{-1} to 1580 cm^{-1} is assigned to C=C from unoxided graphite domains. The peaks at 1369 cm^{-1}, 1220 cm^{-1}, and 1122 cm^{-1} can be assigned to the streching vibrations from C–OH, epoxy, and C—O, respectively.[25–28] After reduction with hydrazine, the peaks at around 3600 cm^{-1} to 3000 cm^{-1} and 1662 cm^{-1} disappeared. Moreover, compared with GO, the intensities of the peaks associated with oxygen functional groups decreased significantly, which indicated that the hydroxyl groups of GO can be removed more effectively than the oxygen functional groups of GO (carbonyl

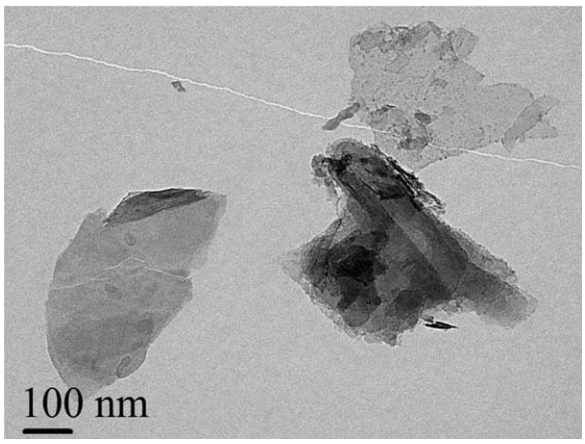

Figure 2. TEM image of GNSs.

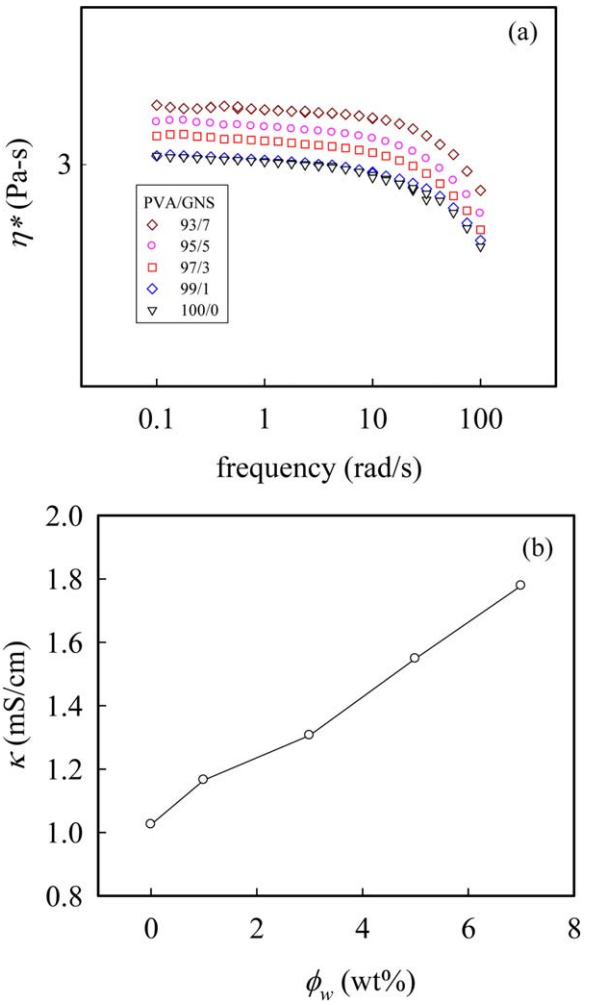

Figure 3. Effects of GNS concentration on (a) solution viscosity and (b) solution conductivity at 25°C. [Color figure can be viewed in the online issue, which is available at wileyonlinelibrary.com.]

and epoxy groups) in our reduction system at pH 10.6. A similar result has been reported by Fernández-Merino *et al.*[27]

The morphology of GNSs was characterized via TEM. Figure 2 shows the deposited GNS structure on the TEM grid prepared from water/SDBS solution. The GNS exhibits a lateral dimension of 500nm × 300 nm, which is due to the small dimension of graphite (1000 mesh). In addition, some GNSs appeared darker, which indicates that several small fragments of graphene were stacked together. Dispersion of nonpolar GNS in the polymer matrix without re-stacking together is the key to determine composite performance. According to Zhao *et al.*,[18] SDBS can be adsorbed onto GNS to avoid GNS aggregation. Therefore, the lyophilized GNSs were re-dispersed in water via sonication with the use of the ionic surfactant, SDBS, and PVA/GNS solution was then prepared by adding PVA powders.

Effect of GNS Filler on Solution Properties

In general, for solutions with a concentration lower than entanglement concentration (C_e), electrospinning is eventually degenerated to electrospraying. To produce uniform fibers via electrospinning, the solution concentration should be as large as 1.8~2.5 C_e.[29,30] In addition, Koski *et al.*[31] have shown that beaded fibers were obtained during electrospinning for 6 wt % PVA (M_w = 124,000 g/mol to 186,000 g/mol, solution entanglement number = 1.95[32]) solution. Based on the method proposed by McKee *et al.*,[29] the log–log plot of the solution's specific viscosity versus volume fraction was constructed to determine the C_e for the present PVA/water solutions. The rapid viscosity increase at ~4 wt % suggested the existence of a chain entanglement occurring around this concentration (Supporting Information Figure S2). Therefore, we selected 10 wt % PVA solution to ensure completely stable fiber formation during electrospinning.

Different amounts of GNS were added into the 10 wt % PVA solution, which can be used to obtain smooth PVA nanofibers via electrospinning. Figure 3a shows the complex viscosity (η^*) of PVA solutions filled with different amounts of GNSs at 25°C. For the neat PVA solution, Newtonian flow behavior occurs at low frequencies, and the behavior then becomes non-Newtonian at frequencies higher than 7 rad/s. Moreover, for the neat PVA solution, the value of zero shear viscosity (η_o) curves is 3.04 Pa-S. When the GNS content was increased to 7 wt %, the value of η_o reached 3.33 Pa-S and the η^* of GNS-filled solution slightly increased without changing the curve shape. Compared with the viscosities observed from PA/CNC[33] and PDLLA/CNC[34] composite solutions, the PVA/GNS composite solution exhibited Newtonian instead of non-Newtonian flow at low frequencies. This finding indicates that the PVA/GNS composite solution did not form GNS–PVA networks. Figure 3b shows the solution conductivity of the PVA solution filled with GNS. For the neat PVA solution, the measured κ is 1.03 mS/cm. Given that GNSs are conductive fillers, adding GNSs into PVA solutions significantly improves κ values. After adding 7 wt % GNSs to the PVA solution, the measured κ is 1.78 mS/cm, which is significantly higher (73%) compared with that of the neat PVA

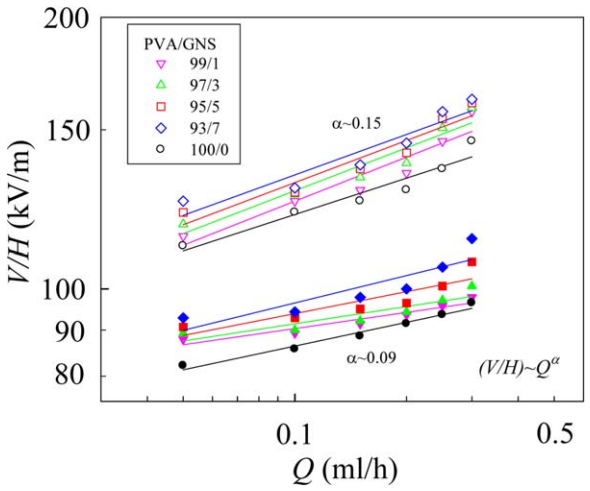

Figure 4. Functional domain for electrospinning of 10 wt % PVA solution with various GNS contents. The domains indicate the range of operating electric fields required for the stable cone-jet mode. (Filled symbols for lower bond electric fields and open symbols for upper bond electric fields). [Color figure can be viewed in the online issue, which is available at wileyonlinelibrary.com.]

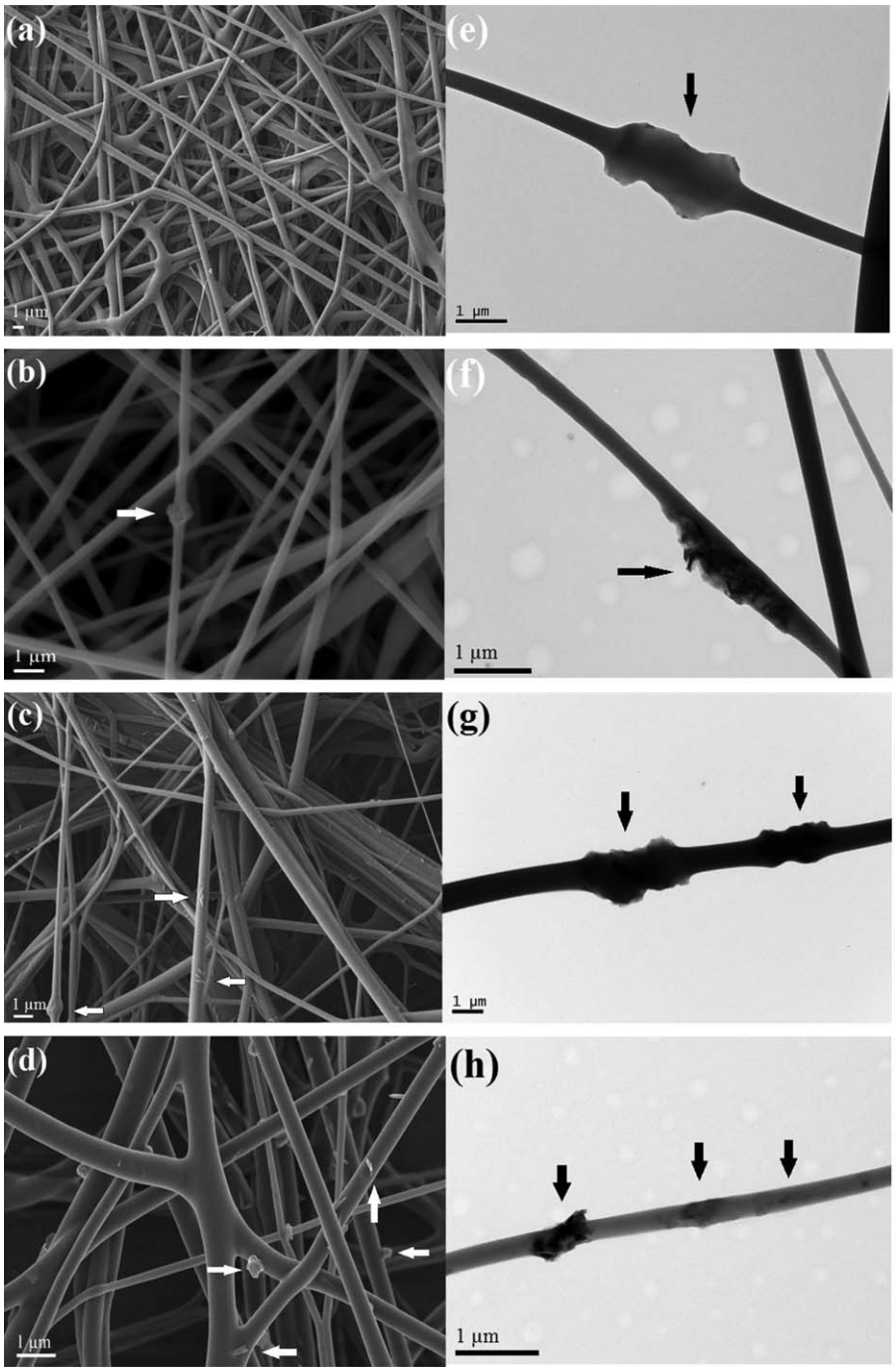

Figure 5. SEM images of electrospun mat obtained from 10 wt % PVA solutions filled with different amounts of GNSs. SEM images of electrospun PVA nanofibers filled with (a) 1 wt %, (b) 3 wt %, (c) 5 wt %, and (d) 7 wt % GNS. TEM images of electrospun PVA nanofibers filled with (e) 1 wt %, (f) 3 wt %, (g) 5 wt %, and (h) 7 wt % GNS ($Q = 0.2$ mL/h, $H = 14$ cm, and $V = 15$ kV). The positions of GNS are indicated by the arrows.

solution. This result indicates that the addition of GNS in PVA solution can significantly increase the conductivity of the PVA solution.

Figure 4 shows the functioning domain for electrospinning 10 wt % PVA solution with various GNS contents. Functioning domains[35,36] are defined as the operating windows of electric field and flow rates that are required for a stable cone-jet mode. The lower- and upper-bound electric fields are denoted as V_s and V_{us}, respectively. Given the volatility of the water solvent, a working distance (H) of 14 cm was used. At a given Q, the operating windows ($V_{us} - V_s$) are higher for the PVA solution filled with GNS content than that for the neat PVA solution. Moreover, increasing the GNS contents also increases the operating windows at a given Q. Wang *et al.*[37] showed that a scaling law of $(V/H) \sim Q^{\alpha}$ can be constructed to characterize the electric field for a stable cone-jet mode. The determined exponent

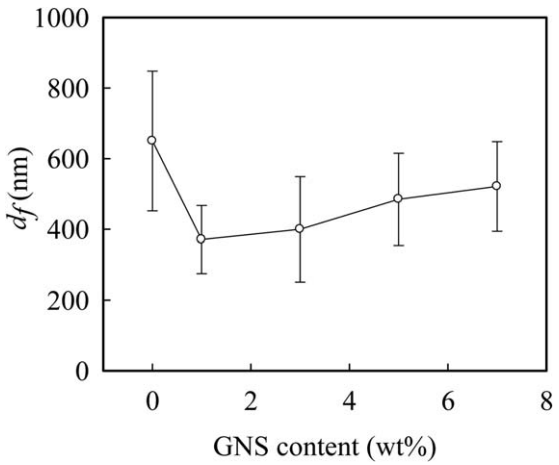

Figure 6. Fiber diameter versus GNS content of PVA/GNS nanofiber.

α is in the range of 0.09 to 0.15 for the PVA solutions with various amounts of GNS. Based on the functioning domain for electrospinning PVA/GNS solutions (Figure 4), a common but limited processing window does exist to determine the effect of GNSs. Therefore, the determined Q and V are 0.2 mL/h and 15 kV in electrospinning the PVA/GNS solution to demonstrate the effects of GNS on fiber diameter.

Effect of GNS Concentration on Electrospinning and As-Spun Fiber Morphology

To determine the effect of GNS addition on fiber morphology and diameter, 10 wt % PVA solutions filled with 1–7 wt % GNSs were electrospun and compared. Figure 5 shows the SEM and TEM images of the nanofiber collected from electrospinning 10 wt % PVA solutions with various amounts of GNS at conditions of Q = 0.2 mL/h, H = 14 cm, and V = 15 kV. The arrows indicate the position of GNSs. Based on SEM micrographs shown in Figures 5(a–d), the PVA composite nanofibers became less smooth and formed an increasingly irregular structure along the fiber with increasing amount of GNS. As shown in Figures 5(e–g), GNSs are identifiable in the TEM images. The GNS particles slightly protrude from the smooth PVA nanofiber. When the GNS content in the PVA solution was increased, several GNSs aggregated during electrospinning, and a small protrusion of these aggregates was observed on the fiber surface. Although the addition of SDBS in the prepared PVA/GNS solution prevents GNS aggregation, several GNSs were still slightly aggregated. When the GNS content reached 7 wt %, GNSs were more distinctly distributed in the PVA nanofiber, and the distance between GNSs became smaller (Figure 5h).

PVA/GNS fiber diameters were measured using a collection of over 200 fibers. Figure 6 shows the fiber diameter of PVA/GNS composite nanofiber filled with GNS at the same electrospinning condition (Q = 0.2 mL/h, H = 14 cm, and V = 15 kV). For neat PVA nanofiber, the measured d_f is 650 ± 198 nm. When GNS content was increased to 1 wt %, the d_f of PVA/GNS 99/1 nanofiber decreased significantly to 371 ± 96 nm. However, when GNS content was further increased to 7 wt %, the d_f of PVA/GNS 93/7 nanofiber slightly increased to 521 ± 127 nm. The d_f of PVA/GNS fiber initially decreased and then increased with increasing GNS content. In electrospinning, solution viscosity and conductivity are important parameters in determining the d_f of electrospun fibers. In the previous studies,[38,39] d_f decreased with decreasing solution viscosity and increasing solution conductivity. Based on the results in Figure 3b, the solution conductivity of PVA/GNS solutions increased with increasing GNS content. High solution conductivity is the main cause of the decrease in d_f of PVA/GNS composite nanofibers because higher solution conductivity induces higher electrostatic force during electrospinning process. This finding is in agreement with those in previous studies.[13,40] Furthermore, based on the results in Figure 3a, the solution viscosity of the PVA/GNS solution also slightly increased with increasing GNS

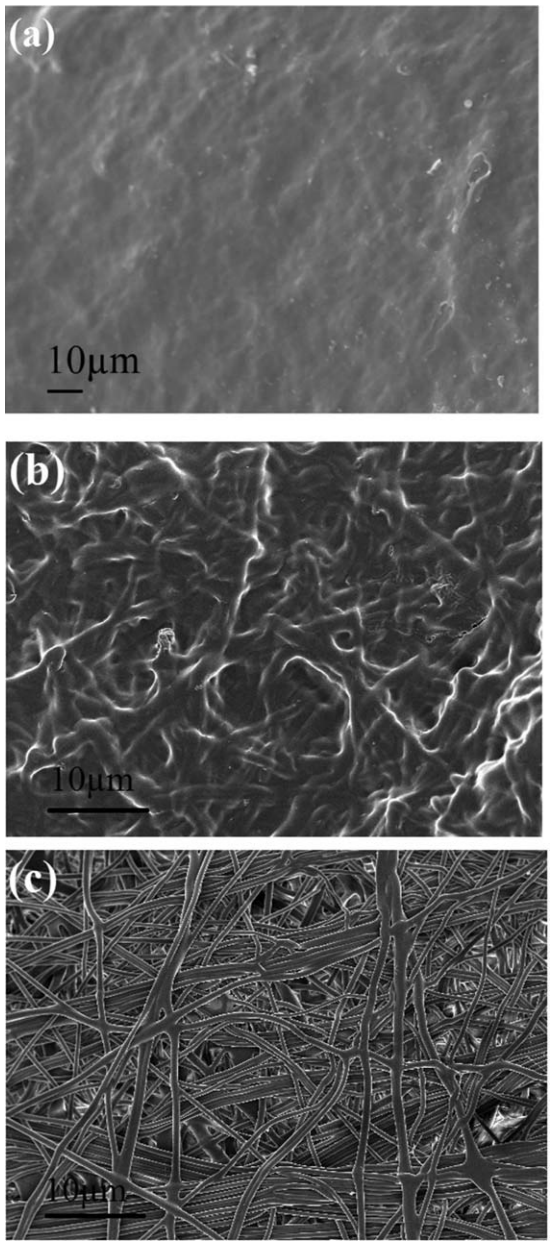

Figure 7. SEM images of the (a) as-spun, (b) methanol-treated, and (c) thermally treated PVA/GNS nanofibers after water immersion at 37°C water for one day.

content. This phenomenon results in a slight increase in the d_f of PVA/GNS composite nanofiber, when GNS content was further increased. Therefore, the change in d_f is attributed to the larger increase in solution conductivity than that in solution viscostiy.

Characterization of Electrospun PVA/GNS Composite Fiber

Figure 7a shows the SEM images of the as-spun PVA/GNS nanofiber after water immersion at 37°C for one day. The PVA/GNS fiber mats were transformed into a thin film without any fiber structure. However, PVA can be physically cross-linked via crystallization without covalent cross-linking. Two kinds of methods can be employed to increase PVA crystallinity. One method is by immersing PVA in methanol. Thus, PVA/GNS nanofibers were immersed in methanol solution at room temperature for one day and then were put in the vacuum oven at 50°C for one day to remove the residual methanol. Figure 7b shows the SEM images of PVA/GNS nanofibers subjected to methanol treatment and then immersed in water at 37°C for one day. The fiber structures do not fully disappear, and some fibers merge with the others. Based on the study of Yao *et al.*,[41] PVA nanofibers can be physically cross-linked via methanol treatment because the crystallinity increases. The group assumed that the crystallinity of PVA nanofibers increases because of the increase in intermolecular polymer hydrogen bonding via the removal of residual water within the fiber by methanol. Similar results have also been reported in a PVA/Ag nanofiber system by Hong *et al.*[11] Another method involves the thermal treatment of PVA by cold crystallization. The PVA/GNS nanofibers were heated to 190°C at 10°C/min and held at 190°C for 15 min to crystallize the PVA chain in the hot stage. The nanofibers were subsequently cooled to room temperature at 10°C min^{-1}. After thermal treatment, the color of the PVA/GNS nanofiber mats changed from gray to light brown. Figure 7c shows the SEM images of PVA/GNS nanofibers via thermal treatment after water immersion at 37°C for one day. The fiber structures are significantly maintained in water. Thus, PVA/GNS nanofibers via thermal treatment can more successfully preserve the fiber structure in water than that via methanol treatment, which is similar to the study of Hong *et al.*[11]

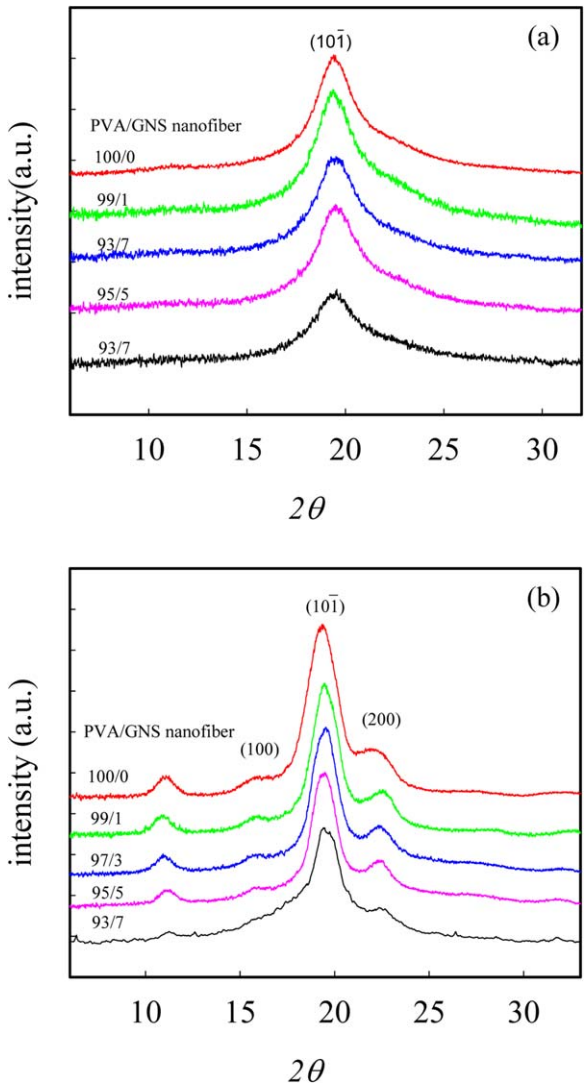

Figure 8. WAXD intensity profiles of the (a) as-spun and (b) thermally treated PVA/GNS nanofibers. [Color figure can be viewed in the online issue, which is available at wileyonlinelibrary.com.]

Figure 8 shows the WAXD intensity profiles for the as-spun PVA/GNS nanofibers and thermally treated PVA/GNS nanofibers. The diffraction peak at 26° related with the *d*-spacing of the graphitic structure was not detected for PVA/GNS composite nanofibers. Thus, GNSs may not stick together again after reduction with hydrazine and are dispersed well in PVA composite nanofibers. For the as-spun neat PVA nanofibers (Figure 8a), a crystalline structure was detected with a strong peak at $2\theta = 19.4°$ (10$\bar{1}$).[42] During electrospinning, the PVA crystalline phase was readily developed in the composite nanofibers. After adding GNS (1–7 wt %), the PVA/GNS composite nanofiber retained PVA crystals with a pseudo-orthorhombic structure. Moreover, after the deconvolution of diffraction curves, the crystalline fraction of the as-spun PVA/GNS nanofiber (χ_a) was estimated from the ratio of integrated intensities from all crystalline peaks to the total intensity curve. As shown in Table I, the as-spun PVA/GNS nanofibers exhibited a maximum χ_a of 0.33 for the 1 wt % GNS content. In addition, when GNS content was lower than 5 wt %, the χ_a of PVA/GNS fibers almost remained constant. However, χ_a decreased to 0.24 with the increase in GNS content to 7 wt %. Based on Figure 8b, for PVA/GNS nanofibers heated to 190°C, a major crystalline peak was found at $2\theta = 19.4°$ (10$\bar{1}$), as well as two shoulders at $2\theta =$ 16.1(001) and 22.7° (200).[42–44] After the deconvolution of diffraction curves, the determined crystalline fractions of PVA/GNS nanofibers with thermal treatment (χ_t) are listed in Table I. Thermally treated PVA/GNS nanofibers also exhibited a maximum χ_t of 0.56 for the sample with 1 wt % GNS content. χ_t decreased to 0.37 with the increase in GNS content to 7 wt %. With the addition of GNS into PVA fibers, the crystallinity of thermally treated PVA/GNS fiber also decreased at higher GNS contents. After thermal treatment, χ_t became higher than χ_a. This finding indicates that the crystallinity of the thermally treated PVA/GNS fibers increased significantly. Therefore, thermally treated PVA/GNS nanofiber can stabilize PVA fiber structures against disintegration in water Figure 7c. Nevertheless,

Table I. Crystalline Properties of the Electrospun Nanofibers Obtained from 10 wt % PVA Solution with Different Amounts of GNS

Sample code	χ_a	χ_t	T_c (°C)	T_{m1} (°C)	T_{m2} (°C)	$\Delta H'_m$ (J/g)
100/0	0.31	0.54	191.1	223.0	225.5	57.0
99/1	0.33	0.56	194.7	222.7	226.4	63.4
97/3	0.31	0.46	196.2	224.6	226.7	60.7
95/5	0.28	0.45	196.7	222.4	225.6	56.8
93/7	0.24	0.37	197.7	220.7	-	58.9

when GNS content is higher than 5 wt %, the distance between GNS in PVA fiber can become smaller and then aggregate, thereby retarding regular PVA crystalline lamellae growth during thermal treatment. This finding is in good agreement with that in the study of Zhao *et al.*[18]

Figure 9a shows the DSC heating traces of GNS-filled fibers. Figure 9b shows the subsequent cooling curves, which reveal the nucleating effects of GNSs on the crystallization of PVA from the melt state. Melting peak temperature, crystallization peak temperature, and endothermic enthalpy are denoted as T_{m1}, T_{m2}, T_c, and ΔH_m, respectively, which are listed in Table I. Neat PVA showed two melting peaks (T_{m1} and T_{m2}) of 223.0°C and 225.5°C, respectively. Given that PVA crystals exhibit only one modification, the double melting peaks should not be attributed to PVA modification. In addition, the possibility of melting/recrystallization/remelting event during DSC heating scan is also ruled out because the lack of relevant literature reports. We speculate that phase separation occurs in the PVA solution and during electrospinning process to render the compelling morphologies conserved in the as-spun PVA fibers. Komatsu *et al.*[45,46] have pointed out that PVA phase separation by spinodal decomposition occurs, but the solution does not change into a gel. In addition, phase separation may also take place during electrospinning process, which is presumably caused by an increased polymer concentration in the whipping jet when fibers are formed and the "evaporation cooling" effects of the electrospinning jet.[47] Therefore, the PVA solution may separate into PVA-rich and PVA-poor domains, which could result in two different crystallite sizes during DSC heating scan. Shenoy *et al.*[32] have demonstrated that the electrospun PVA fiber formed at low solution entanglement number (< 1) conduction, which is caused by the phase separation in the PVA solution.

When the GNS content was lower than 5 wt %, the T_{m1} and T_{m2} of PVA/GNS fibers almost remained constant. However, when the GNS content was increased to 7 wt %, T_{m1} slightly decreased to 220.7°C, and T_{m2} disappeared. In addition, the melting curve shifted to the low-temperature region. This phenomenon indicates that the presence of high GNS contents in the PVA solution retards the phase separation process and yields PVA lamellae with small thicknesses in the as-spun fibers. To compare the amount of melting crystals, ΔH_m was normalized with the PVA content to derive $\Delta H'_m[=\Delta H_m/(1-\phi_w)]$. The $\Delta H'_m$ of the PVA/GNS nanofiber increased with increasing GNS from 57.0 J/g, for the neat PVA nanofiber, to 63.4 J/g, for nanofibers filled with 1 wt % GNS. $\Delta H'_m$ slightly decreased for GNS higher than 1 wt %. The DSC results are consistent with WAXD results. Furthermore, Morimune *et al.*[48] found no significant increase in the T_m and the crystallinity of the composites with increasing GO content by studying the dynamic crystallization of the PVA/GO composites. In addition, Dassios *et al.*[49] demonstrated that the T_m of PVA/CNT composite nanofibers was higher than that of neat PVA nanofiber. Furthermore, clay has a two-dimensional layered structure similar to GNS, which is composed of one or more clay minerals. Strawhecker *et al.*[50]

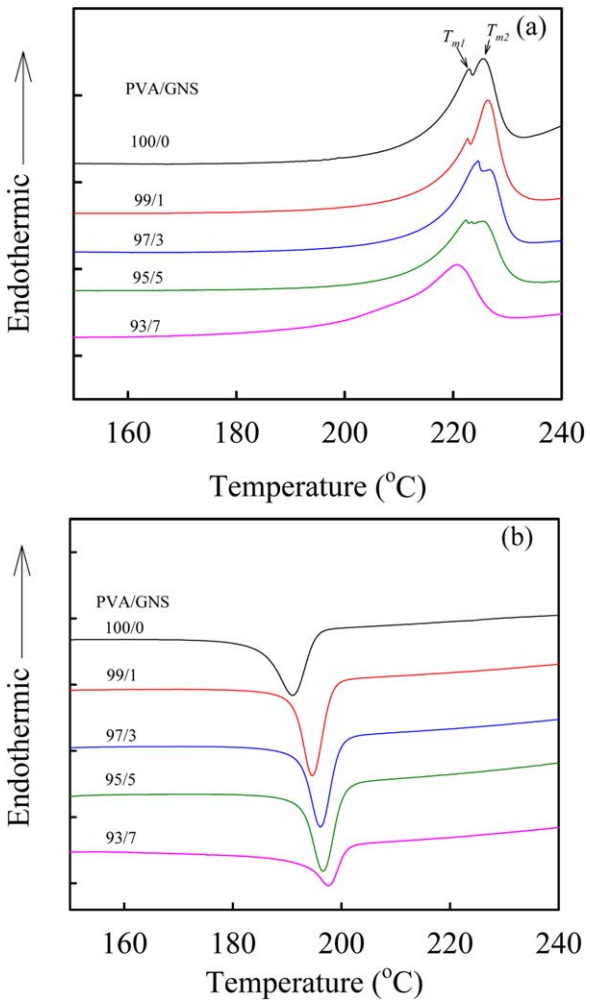

Figure 9. DSC (a) heating and (b) cooling traces of electrospun PVA fibers from 10 wt % solutions with different GNS contents. [Color figure can be viewed in the online issue, which is available at wileyonlinelibrary.com.]

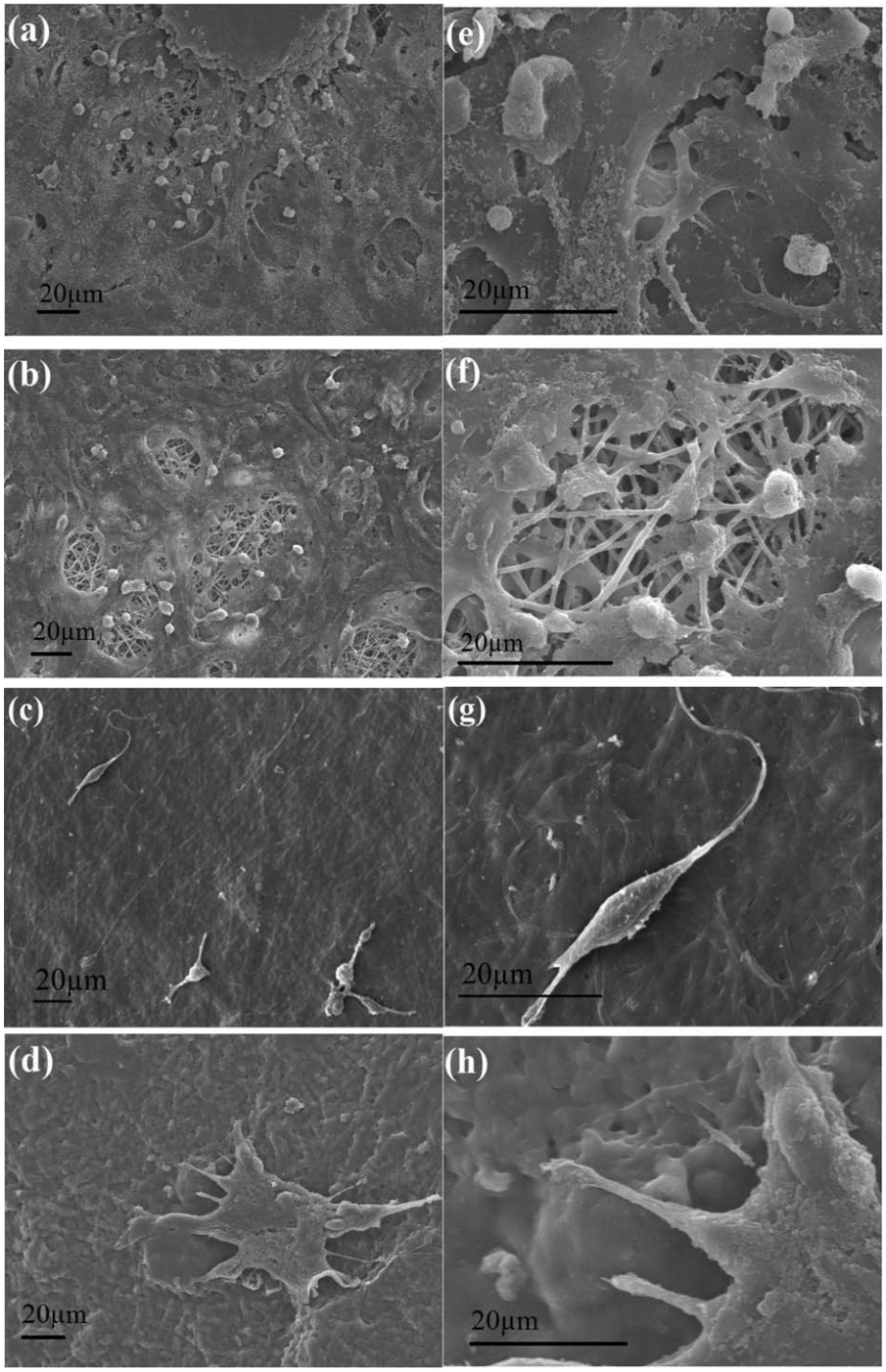

Figure 10. SEM images of fibroblast cells attached and grown on the surfaces of (a) neat thermally treated PVA nanofiber mats, (b) thermally treated PVA/GNS 95/5 nanofiber mats, (c) methanol-treated neat PVA nanofiber mats, and (d) methanol-treated PVA/GNS 95/5 nanofiber mats after 72-h incubation. (e), (f), (g), and (h) show the enlarged SEM images (5x) in (a), (b), (c), and (d), respectively.

also found that the presence of clays in PVA composites resulted in a higher melting temperature phase and that the T_m of PVA increased with increasing clay content. However, given the phase separation of PVA solution and the effect of GNS addition at high content, GNS had little effect on the PVA crystallites size of PVA/GNS nanofibers. This finding indicates that the crystallite sizes of PVA/GNS nanofibers are not similar with those of PVA/GNS composites films.

Compared with neat PVA sample melt-crystallized at 191.1°C, PVA melt filled with 1 wt % GNS had an increase in T_c by 3.3°C (Figure 9b). When GNS content was increased to 7 wt %, T_c slightly increased to 197.7°C. In other words, the melted crystallization rate of PVA chains in the GNS-filled composite nanofiber increased with increasing GNS content. This finding is in agreement with the PVA/GNS composite study of Lee *et al.*[51] The group proved that GNS functions as an effective nucleating agent

during the crystallization process at low content, thereby increasing the degree of crystallinity and crystallization rate. Therefore, the addition of GNSs may influence the melt-crystallization behavior of PVA nanofibers and may also exhibit a similar melt-crystallization behavior with PVA/GNS composites film.

Morphology of Cells Cultured onto PVA/GNS Nanofiber Scaffolds

Based on the above results, GNSs protrude from the fibers, but the crystallinity of the PVA/GNS fiber decreases in higher GNS content, especially 7 wt % GNSs. Protruded GNSs in PVA scaffolds presents particular advantage such as enhancing antibacterial properties and accelerating cell differentiation.[2,15] Therefore, the scaffold (used in this study) for cell culture is composed of 95/5. Figure 10 shows several typical SEM micrographs of morphological analyses. These images reveal the different treatments for PVA/GNS nanofiber mats on the proliferative morphologies of 3T3 cells after 72-h incubation. Based on the SEM micrographs shown in Figures 10(a,b,e,f), 3T3 cells initially displayed a spider shape on neat PVA and PVA/GNS scaffolds. The nanofiber morphologies of the thermally treated scaffolds were maintained after 72 h of culture of 3T3 cells on the surfaces of scaffolds. Fibroblasts were extended and evenly distributed over the surface, which indicate that 3T3 cells acted well on the porous surface of PVA nanofiber scaffolds. Moreover, cellular activities such as adhesion to PVA/GNS scaffolds are similar to that in neat PVA scaffolds. Based on the SEM micrographs shown in Figures 10(c,d,g,h), the nanofiber morphologies of scaffolds subjected to methanol treatment were not preserved well after immersion in the culture medium for 72 h. 3T3 cells displayed a spindle shape on neat PVA scaffolds, and only a few cells were attached on the surface. When PVA scaffolds were subjected to methanol treatment, the porous structures on the scaffold disappeared and became flat. Fibroblasts had the tendency to grow or adhere on the flat surface, but only a few cells were attached on the surface even after 72 h of cell culture. Thus, PVA scaffolds that were treated with methanol are cytotoxic.

Notably, when the GNSs were effectively incorporated into PVA scaffolds, 3T3 cells displayed spider shape with better adhesion. Thus, GNSs can slightly reduce the cytotoxic effect of methanol-treated PVA scaffolds. This finding is in agreement with those in previous studies. [2,13] Accordingly, the thermally treated PVA/GNS scaffold shows better performance of 3T3 cells in terms of adhesion and proliferation than scaffolds treated with methanol.

CONCLUSIONS

GNS powder with small lateral dimension was successfully obtained via chemical reduction and lyophilization. An effective surfactant, SDBS, was used to prepare PVA composite nanofiber filled with well-dispersed GNSs via electrospinning. The effects of increasing GNS concentration on the electrospinning solution and process, as well as the morphologies and property variations of PVA/GNS composite nanofibers, were investigated using several analytical techniques, including rheometer, conductivity meter, DSC, WAXD, SEM, and TEM. The addition of GNSs increased the viscosity and conductivity of the PVA soution. For electrospinning 10 wt % PVA solution with various GNS content, the d_f of PVA/GNS fibers initially decreases and then increases with the addition of GNSs into PVA solution. The decrease in d_f of the PVA/GNS fiber is initially dominated by solution conductivity, and the increase in d_f of the PVA/GNS fiber is dominated by solution viscosity. The change in d_f is attributed to the larger increase in solution conductivity than that in solution viscosity. GNSs are embedded in the fibers and protrude from the fibers. After thermal treatment, the crystallinity of thermally treated PVA/GNS nanofibers is higher than that of as-spun PVA/GNS nanofibers. In addition, thermally treated PVA nanofibers can stabilize fiber structures against disintegration in water. The crystallinity of the PVA/GNS fiber decreases at higher GNS content. For tissue engineering application, GNSs can slightly reduce the cytotoxic effect of methanol-treated PVA scaffolds. The thermally treated PVA/GNS scaffold exhibits better performances for 3T3 cells in terms of adhesion and proliferation than the scaffold treated with methanol.

ACKNOWLEDGMENTS

The authors are grateful to the National Science Council of Taiwan (ROC) for the research grant (NSC 101-2218-E-035-006-) that supported this work. We thank Prof. C. Wang in NCKU for the valuable discussions on electrospun nanofibers.

REFERENCES

1. Cui, W.; Zhou, Y.; Chang, J. *Sci. Technol. Adv. Mater.* **2010**, *11*, 014108.
2. Lu, B.; Li, T.; Zhao, H.; Li, X.; Gao, C.; Zhang, S.; Xie, E. *Nanoscale* **2012**, *4*, 2978.
3. Song, W.; Markel, D. C.; Wang, S.; Shi, T.; Mao, G.; Ren, W. *Nanotechnology* **2012**, *23*, 115101.
4. Wang, X.; Xie, X.; Cai, C.; Rytting, E.; Steele, T.; Kissel, T. *Macromolecules* **2008**, *41*, 2791.
5. Chiellini, E.; Corti, A.; D'Antone, S.; Solaro, R. *Prog. Polym. Sci.* **2003**, *28*, 963.
6. Matsumura, S.; Tomizawa, N.; Toki, A.; Nishikawa, K.; Toshima, K. *Macromolecules* **1999**, *32*, 7753.
7. Zhang, C.; Yuan, X.; Wu, L.; Han, Y.; Sheng, J. *Eur. Polym. J.* **2005**, *41*, 423.
8. Peresin, M. S.; Habibi, Y.; Zoppe, J. O.; Pawlak, J. J.; Rojas, O. J. *Biomacromolecules* **2010**, *11*, 674.
9. Kurihara, S.; Sakamaki, S.; Mogi, S.; Ogata, T.; Nonaka, T. *Polymer* **1996**, *37*, 1123.
10. Gao, L.; Seliskar, C. *J. Chem. Mater.* **1998**, *10*, 2481.
11. Hong, K. H.; Park, J. L.; Sul, I. H.; Youk, J. H.; Kang, T. J. *J. Polym. Sci. Polym. Phys.* **2006**, *44*, 2468.
12. Naebe, M.; Lin, T.; Staiger, M. P.; Dai, L.; Wang, X. *Nanotechnology* **2008**, *19*, 305702.
13. Qi, Y.; Tai, Z.; Sun, D.; Chen, J.; Ma, H.; Yan, X.; Liu, B.; Xue, Q. *J. Appl. Polym. Sci.* **2013**, *127*, 1885.
14. Novoselov, K. S.; K., G. A.; Morozov, S. V.; Jiang, D.; Zhang, Y.; Dubonos, S. V.; Grigorieva, I. V.; Firsov, A. A. *Science* **2004**, *306*, 666.

15. Nayak, T. R.; Andersen, H.; Makam, V. S.; Khaw, C.; Bae, S.; Xu, X.; Ee, P. L. R.; Ahn, J. H.; Hong, B. H.; Pastorin, G. *ACS Nano* **2011**, *5*, 4670.
16. Veca, L. M.; Lu, F.; Meziani, M. J.; Cao, L.; Zhang, P.; Qi, G.; Qu, L.; Shrestha, M.; Sun, Y. P. *Chem. Commun.* **2009**, 2565.
17. Vadukumpully, S.; Paul, J.; Valiyaveettil, S. *Carbon* **2009**, *47*, 3288.
18. Zhao, X.; Zhang, Q.; Chen, D.; Lu, P. *Macromolecules* **2010**, *43*, 2357.
19. Das, S.; Wajid, A. S.; Shelburne, J. L.; Liao, Y. C.; Green, M. J. *ACS Appl. Mater. Interfaces* **2011**, *3*, 1844.
20. Das, S.; Wajid, A. S.; Bhattacharia, S. K.; Wilting, M. D.; Rivero, I. V.; Green, M. J. *J. Appl. Polym. Sci.* **2013**, *128*, 4040.
21. Hummers Jr, W. S.; Offeman, R. E. *J. Am. Chem. Soc.* **1958**, *80*, 1339.
22. Cao, Y.; Feng, J.; Wu, P. *Carbon* **2010**, *48*, 3834.
23. Huang, C. L.; Peng, S. Y.; Wang, Y. J.; Chen, W. C.; Lin, J. H. *Appl. Mech. Mater.* **2013**, *365*, 1025.
24. Zhang, J.; Zou, H.; Qing, Q.; Yang, Y.; Li, Q.; Liu, Z.; Guo, X.; Du, Z. *J. Phys. Chem. B* **2003**, *107*, 3712.
25. Si, Y.; Samulski, E. T. *Nano Lett.* **2008**, *8*, 1679.
26. Ren, P. G.; Yan, D. X.; Ji, X.; Chen, T.; Li, Z. M. *Nanotechnology* **2011**, *22*, 055705.
27. Fernández-Merino, M.; Guardia, L.; Paredes, J.; Villar-Rodil, S.; Solis-Fernandez, P.; Martinez-Alonso, A.; Tascon, J. *J. Phys. Chem. C* **2010**, *114*, 6426.
28. Marcano, D. C.; Kosynkin, D. V.; Berlin, J. M.; Sinitskii, A.; Sun, Z.; Slesarev, A.; Alemany, L. B.; Lu, W.; Tour, J. M. *ACS Nano* **2010**, *4*, 4806.
29. McKee, M. G.; Wilkes, G. L.; Colby, R. H.; Long, T. E. *Macromolecules* **2004**, *37*, 1760.
30. Shenoy, S. L.; Bates, W. D.; Frisch, H. L.; Wnek, G. E. *Polymer* **2005**, *46*, 3372.
31. Koski, A.; Yim, K.; Shivkumar, S. *Mater. Lett.* **2004**, *58*, 493.
32. Shenoy, S. L.; Bates, W. D.; Wnek, G. *Polymer* **2005**, *46*, 8990.
33. Tsou, S. Y.; Lin, H. S.; Cheng, P. J.; Huang, C. L.; Wu, J. Y.; Wang, C. *Eur. Polym. J.* **2013**, *49*, 3619.
34. Chien, H. S.; Wang, C. *J. Appl. Polym. Sci.* **2013**, *128*, 958.
35. Cloupeau, M.; Prunet-Foch, B. *J. Electrostat.* **1989**, *22*, 135.
36. Chen, D. R.; Pui, D. Y.; Kaufman, S. L. *J. Aerosol Sci.* **1995**, *26*, 963.
37. Wang, C.; Cheng, Y. W.; Hsu, C. H.; Chien, H. S.; Tsou, S. Y. *J. Polym. Res.* **2011**, *18*, 111.
38. Bhattarai, S. R.; Bhattarai, N.; Yi, H. K.; Hwang, P. H.; Cha, D. I.; Kim, H. Y. *Biomaterials* **2005**, *25*, 2595.
39. Wang, C.; Hsu, C. H.; Lin, J. H. *Macromolecules* **2006**, *39*, 7662.
40. Ahn, B. W.; Chi, Y. S.; Kang, T. J. *J. Appl. Polym. Sci.* **2008**, *110*, 4055.
41. Yao, L.; Haas, T. W.; Guiseppi-Elie, A.; Bowlin, G. L.; Simpson, D. G.; Wnek, G. E. *Chem. Mater.* **2003**, *15*, 1860.
42. Mooney, R. C. *J. Am. Chem. Soc.* **1941**, *63*, 2828.
43. Assender, H. E.; Windle, A. H. *Polymer* **1998**, *39*, 4295.
44. Ricciardi, R.; Auriemma, F.; De Rosa, C.; Lauprêtre, F. *Macromolecules* **2004**, *37*, 1921.
45. Kawanishi, K.; Komatsu, M.; Inoue, T. *Polymer* **1987**, *28*, 980.
46. Komatsu, M.; Inoue, T.; Miyasaka, K. *J. Polym. Sci. Polym. Phys.* **1986**, *24*, 303.
47. Megelski, S.; Stephens, J. S.; Chase, D. B.; Rabolt, J. F. *Macromolecules* **2002**, *35*, 8456.
48. Morimune, S.; Kotera, M.; Nishino, T.; Goto, T. *Carbon* **2014**, *70*, 38.
49. Dassios, K. G.; Galiotis, C. *Carbon* **2012**, *50*, 4291.
50. Strawhecker, K.; Manias, E. *Chem. Mater.* **2000**, *12*, 2943.
51. Lee, S.; Hong, J. Y.; Jang, J. *Polym. Int.* **2013**, *62*, 901.